New Journal and we have not received input yet 25 (2021) 101044

Contents lists available at ScienceDirect

Thermal Science and Engineering Progress

journal homepage: www.sciencedirect.com/journal/thermal-science-and-engineering-progress

Heat transfer of chemically reacting mixed convection fluid using convective surface condition: Non-Darcy model

J.C. Umavathi [a], Bernardo Buonomo [b], Oronzio Manca [b], Mikhail A. Sheremet [c,*]

[a] Department of Mathematics, Gulbarga University, Gulbarga 585 106, Karnataka, India
[b] Dipartimento di Ingegneria, Università degli Studi della Campania "Luigi Vanvitelli", Via Roma 29, 81031 Aversa, CE, Italy
[c] Laboratory on Convective Heat and Mass Transfer, Tomsk State University, 36 Lenin Avenue, 634050 Tomsk, Russia

ARTICLE INFO

Keywords:
Darcy-Forchheimer-Brinkman model
Soret parameter
Runge-Kutta-shooting method

ABSTRACT

This work reports the study of mixed convection of permeable fluid with Robin conditions in the vertical channel including the effects of chemical reactions. The fluid transport is designed by the Darcy-Forchheimer-Brinkman model. The series method is adopted for approximate solutions for governing equations considering the Brinkman number as the perturbation characteristic whose outcomes correspond to magnitudes of Brinkman number less than one. Adopting a numerical scheme followed by fourth order Runge–Kutta algorithm with shooting method, the solutions for bigger magnitudes of the Brinkman number are obtained. The present results for limiting cases are compared with the literature and good agreement is seen. For various values of thermal and mass Grashof numbers, porous parameter, inertial parameter, Darcy number and first order chemical reaction the problem is resolved for the same and distant Biot numbers reflecting the border temperatures symmetric and asymmetric. Finally, the outcomes are tabulated for wall friction parameters, Nusselt and Sherwood numbers for innovated parameters. It is noticed that enhancing buoyancy and dissipations, thermal Grashof number helps to improve the flow rate for all values of Biot number. The Schmidt and Soret parameters can improve concentration patterns. Nusselt number can be improved with thermal Grashof number and Brinkman number and it is dropped with inertia and porous parameters. The solutions have a very good agreement with Zanchini data without mass Grashof number.

Introduction

The buoyancy-induced double diffusive flow past different geometries planted in solid matrix is applicable in engineering and geophysics. Geothermal cavities, heat insulation, contaminant propagation, enhanced oil recovery, phenomena in chemical and nuclear reactors, and underground energy transport are some of the areas of applications.

Darcy's law [1] is used for slow flows. Nakayama et al. [2] claimed that Darcy's law is valid with low velocity and low permeability. At high permeability or at higher flow rates, inertial effects are also important. Modifications of Darcy's law are well-known approaches of Brinkman [3] and Forchheimer [4]. The Brinkman model accounts for the viscous stresses and Forchheimer model narrates for the nonlinear drag effect owing to the porous matrix. Many modern applications are outlined by high flow velocities. Brinkman-Forchheimer model was adopted by Kuznetsov et al. [5] to study the composite channel flow. Bear [6] pointed out that for values of Reynolds number greater than one, the flow will be non-Darcian. Muskat and Flow [7] worked on the inertia effect introducing the Forchheimer term. Umavathi et al. [8,9,10] discussed laminar and transient convection flows in a composite channel. Malashetty et al. [11,12] worked on the flow nature in an inclined duct for immiscible saturated medium using Brinkman model. Prathap Kumar et al. [13] researched using the isoflux or isothermal boundaries for porous medium overlying a fluid layer. Yahya and Saghir [14] analyzed numerically heat transfer performance in flat and circular pipes having porous insert. The Darcy-Brinkman model was used for porous zone. Experimental and numerical analysis of hybrid nanofluid flow in a heat exchanger with porous inserts was performed by Alhajaj et al. [15]. Authors using the Darcy-Brinkman model within porous zones founded that hybrid nanofluid can enhance the energy transport.

In many transport processes, the chemical reaction effects are found in applications such as solar collector, metallurgy, bio-chemical reactor, and combustion engineering units etc. Concentration of foreign material in air or water characterizes possible origin of chemical reactions. Chemical reactions between different materials can generate the heat.

* Corresponding author.
E-mail address: sheremet@math.tsu.ru (M.A. Sheremet).

https://doi.org/10.1016/j.tsep.2021.101044
Received 4 April 2021; Received in revised form 15 August 2021; Accepted 15 August 2021
Available online 21 August 2021

Nomenclature

A	constant
Bi_1, Bi_2	Biot parameters
Br	Brinkman parameter
Sr	Soret parameter
Sc	Schmidt parameter
C_p	Heat capacity
C_f	Forchheimer coefficient
I	dimensionless inertia coefficient
C_1, C_2	reference concentrations of external fluid
C_0	reference concentration
C	concentration
$D(=2L)$	hydraulic diameter
D_m	mass diffusivity of the solute
g	gravity acceleration
GR_T	heat Grashof number
GR_C	concentration Grashof number
h_1, h_2	outside thermal transfer parameters
k	heat conductivity
L	channel size
n	non-negative integer number
Nu_1, Nu_2	Nusselt parameters
p	pressure
$P = p + \rho_0 gX$	difference between the pressure and hydrostatic pressure
Pr	Prandtl number
Re	Reynolds number
Sh_1, Sh_2	Sherwood numbers
R_T	temperature ratio
S	dimensionless characteristic
T	temperature
T_1, T_2	external fluid reference temperatures
T_0	reference temperature
u	non-dimensional velocity along X-axis
$u_n(y)$	non-dimensional function
$\overline{u}$	mean velocity
U	velocity for x-axis
X	streamwise coordinate
y	non-dimensional transverse coordinate
Y	transverse coordinate

Greek Symbols

α	heat diffusivity
β_T	heat expansion parameter
β_C	concentration expansion parameter
ΔT	temperature drop
ΔC	concentration drop
σ	Darcy number
τ_1, τ_2	wall friction coefficients
ε	non-dimensional parameter
θ	non-dimensional temperature
θ_b	non-dimensional bulk temperature
ϕ	normalized concentration
μ	dynamic viscosity
ν	kinematic viscosity
Λ_1	modified heat Grashof number
Λ_2	modified concentration Grashof number
ρ	mass density
ρ_0	density for $T = T_0$

The energy and mass transport in binary units has immense applications in chemical industry. The Dufour and Soret consequences are influential where species are included at a plate in a liquid with a density less than the fenced liquid. It was remarked that diffusion effect was very strong for hydrogen and helium (molecular weight less than air) when compared with carbon dioxide and xenon (molecular weight greater than air). The temperature difference due to buoyancy is increased by injecting the light gases (examples are helium and hydrogen) and therefore the energy transport strength are raised. Therefore, *Nu* is influenced substantially with the presence of Dufour and Soret parameters. Coelho and Silva Telles [16] explored double diffusion in Graetz flow between parallel plates. Bég et al. [17] surveyed the double diffusion for the MHD permeable fluid. He also explained that mass and energy fields were elevated with rise in Dufour and Soret numbers respectively. Two double distribution lattice-Boltzmann models were established by Luo and Xu [18] to simulate the coupled phenomena of double-diffusive mixed convection, solid–fluid conjugate heat transfer and adsorption process in microporous media at the pore scale. The results demonstrated that the intraparticle mass transfer resistance dominated the overall adsorption performance. But the adsorbed amount of the particle was depending on the concentration in flow field around the particle surface. The mixed convection heat transfer combined with thermal radiation of a viscoelastic liquid circulation driven by a porous accelerating sheet under the inclined uniform magnetic field was studied by Mahabaleshwar et al. [19]. They showed that velocity, thermal and concentration boundary layers thicknesses were raised with a growth of the radiation number, where the opposite impact was found for the increasing magnitudes of Prandtl number.

An analysis for axisymmetric boundary layer couple stress fluid flow over a stretching cylinder under the influence of the magnetic field, chemical reaction, Soret and Dufour parameters was carried out by Gajjela and Garvandha [20]. They observed that the couple stress parameter decelerates the axial velocity and accelerates the temperature and concentration fields. Ali et al. [21] described magnetohydrodynamic effects on the transient rotational flow of Maxwell nanofluids. They noticed that the progressing values of magnetic parameter and Deborah number reduced the primary velocity and the magnitude of secondary velocity but temperature and concentration were incremented. The fully developed forced convective heat and mass transfer in a parallel-plate channel occupied by a bidisperse porous medium was investigated by Wang et al. [22] under the Darcy flow model and the constant heat flux boundary condition. They found that an increase in effective thermal conductivity ratio or Biot number leads to an enhancement in the heat transfer rate. Also, an increase in Soret number leads to an increase in dimensionless concentrations in both phases due to the strong mass diffusion of reactants. Convective flow with chemical reaction in a vertical duct using third kind boundary conditions was investigated by Umavathi et al. [23]. The observations made were that the mass Grashof number reduced the velocity at the left border and enhanced at the right border. The temperature distributions were not much influenced by the mass Grashof number for equal Biot parameters whereas, for the opposite case, its effect was very significant at the left border compared to the right one.

Partha et al. [24] debated the Soret-Dufour effects on hydromagnetic convective flow using a non-Darcy model. They proved that the wall mass and energy rates are considerably affected by the Dufour-Soret parameters with stronger magnetic field. Abd El-Aziz [25] researched double diffusion MHD characteristics of free convection past continuously stretching plate. Fairbanks and Wike [26] worked on the diffusion and chemical reactions along a flat plate. Das et al. [27] investigated the double diffusion on the circulation over an impulsively infinite surface. The diffusion due to mass with higher-order chemical reactions along the linearly stretching plate was scrutinized by Andersson et al. [28]. Umavathi et al. [29–32] abstracted the origin of double diffusive

convection in nano suspension within a porous medium. Prathap Kumar et al. [33] also worked on double diffusive convection of nano suspension in a porous material. Recently Umavathi et al. [34] discussed double-diffusive free convection of nanofluid within a confined rectangular duct numerically. The results found were that the velocity was maximum using silver nanoparticles and minimum using diamond nanoparticles. The temperature was high for silicon oxide nanoparticles and low for diamond nanoparticles and opposite effect was obtained for concentration. Yinusa et al. [35] explored the three-dimensional squeezed flow, heat and mass transfer through a rotating channel with coupled Dufour and Soret influences. The parametric studies revealed how an increase in magnetic term and a decrease in squeezing number reduced the velocity profile by approximately 10 percent. Additionally, continuous decrease of Soret number increased the temperature and concentration profiles.

It should be noted that nowadays there are many published papers on nanofluids flow and heat transfer. Thus, Al Kalbani et al. [36] studied numerically natural convection and entropy production of water/copper nanofluid in an inclined chamber under an impact of tilted magnetic field using local thermal non-equilibrium approach. Authors revealed that liquid fraction gives the major contribution to the total entropy production. Saghir and Rahman [37] examined numerically nanofluid flow and energy transport in a complex channel configuration under an influence of Brownian diffusion and thermophoresis. They ascertained that 1% alumina/water nanofluid allows to reduce the pressure drop. Plant and Saghir [38] scrutinized computationally and experimentally alumina/water nanofluid flow and energy transport in a multi-channel system with porous insertions. They found that low concentration of alumina nanoparticles characterizes the energy transport enhancement compared to high nanoadditives volume fraction. Other interesting and useful results were obtained by Bianco et al. [39], Srinivasacharya and Ramana [40], Tayebi et al. [41].

The boundary conditions for temperature can have various form, e.g. constant temperature, constant heal flux or convective heat transport (Robin border restrictions). The Robin border restrictions deal with practical problems. Javeri [42–44] worked on the flow in different channels using convective conditions on the walls. Umavathi et al. [45–51] analyzed the mixed convection with border restrictions of third kind under an impact of source/sink.

In vision of the practical applications for Robin border conditions and double diffusion convection, the aspiration of the present work is to analyze double diffusion for the flow in a vertical avenue for the non–Darcy model.

Mathematical statement

The physical problem reflected in Fig. 1 includes the infinitely long vertical duct with the border temperatures T_1 and T_2, filled with an incompressible permeable fluid. The X-axis corresponds to the axial direction and is directed parallel to gravity force and Y-axis is perpendicular to borders. The vertical duct corresponds to the domain region $-L/2 \le Y \le L/2$. The characteristics of liquid including heat conductivity, viscosity, heat diffusivity, and heat expansion parameter are fixed.

Consider the Boussinesq approximation once can find

$$\rho = \rho_0[\beta_T(T - T_0) - \beta_C(C - C_0)] \tag{1}$$

Hence the conservation of mass is

$$\frac{\partial U}{\partial X} = 0 \tag{2}$$

so that U depends upon Y-coordinate and hence the flow is one-dimension. The motion equations for both axes are written as

$$\beta_T g(T - T_0) + \beta_C g(C - C_0) - \frac{1}{\rho_0}\frac{\partial P}{\partial X} + \nu\frac{d^2U}{dY^2} - \frac{\nu U}{\kappa} - \frac{C_f U^2}{\sqrt{\kappa}} = 0 \tag{3}$$

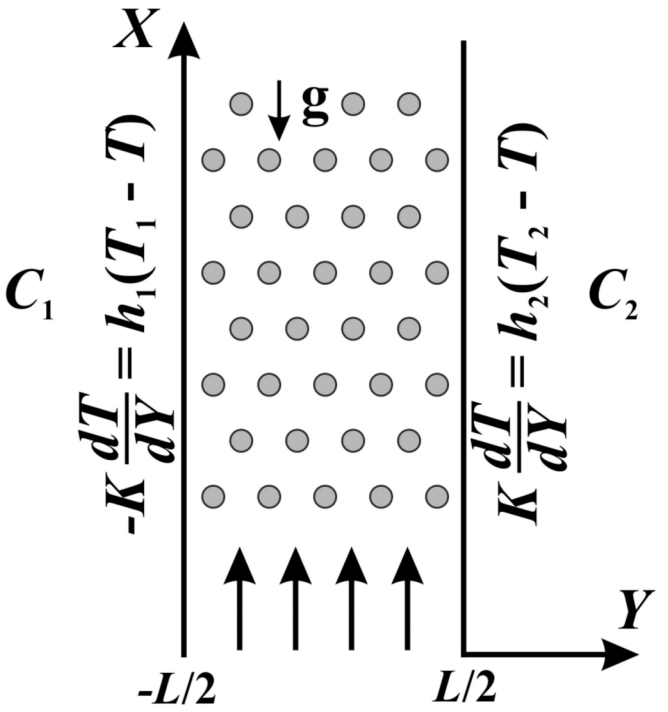

Fig. 1. Schematic diagram.

$$\frac{\partial P}{\partial Y} = 0 \tag{4}$$

From Eq. (4) one can find that P depends upon X-coordinate. Then Eq. (3) implies that

$$(T - T_0) = \frac{1}{\rho_0 g\beta_T}\frac{dP}{dX} - \frac{\mu}{\rho_0 g\beta_T}\frac{d^2U}{dY^2} + \frac{\mu U}{\rho_0 g\beta_T \kappa} - \frac{\beta_C}{\beta_T}(C - C_0) + \frac{C_f U^2}{g\beta_T\sqrt{\kappa}} \tag{5}$$

Differentiating Eq. (5) w. r .to X we get

$$\frac{\partial T}{\partial X} = \frac{1}{\rho_0 g\beta_T}\frac{d^2P}{dX^2} \tag{6}$$

$$\frac{\partial T}{\partial Y} = -\frac{\nu}{g\beta_T}\frac{d^3U}{dY^3} + \frac{\nu}{\kappa g\beta_T}\frac{dU}{dY} - \frac{\beta_C}{\beta_T}\frac{\partial C}{\partial Y} + \frac{C_f}{g\beta_T\sqrt{\kappa}}\frac{dU^2}{dY} \tag{7}$$

$$\frac{\partial^2 T}{\partial Y^2} = -\frac{\nu}{g\beta_T}\frac{d^4U}{dY^4} + \frac{\nu}{\kappa g\beta_T}\frac{d^2U}{dY^2} - \frac{\beta_C}{\beta_T}\frac{\partial^2 C}{\partial Y^2} + \frac{C_f}{\sqrt{\kappa}g\beta_T}\frac{d^2U^2}{dY^2} \tag{8}$$

The walls of the carrier are simulated to be very thin which leads to interchange the energy by convection with the outside liquid. For $Y < -L/2$ the thermal convection is considered to be uniform with h_1 and T_1 to be the uniform reference temperature. For $Y > L/2$ the outside convection parameter is assumed to be h_2 and the fluid region will be have uniform reference temperature T_2 such that $T_2 > T_1$. In addition, C_1 (left) and C_2 (right) are the concentrations at the plates. Therefore the conditions on the temperature filed at the boundaries are

$$-\left[k\frac{\partial T}{\partial Y}\right]_{Y=-L/2} = h_1[T_1 - T(X, -L/2)] \tag{9}$$

$$-\left[k\frac{\partial T}{\partial Y}\right]_{Y=L/2} = h_2[T(X, L/2) - T_2] \tag{10}$$

These equations can be reduced using Eq. (7)

$$\left[\frac{d^3U}{dY^3} - \frac{1}{\kappa}\frac{dU}{dY} - \frac{C_f}{\nu\sqrt{\kappa}}\frac{dU^2}{dY}\right]_{Y=-L/2} = \frac{\beta_T g h_1}{k\nu}\left(1 - \frac{k\beta_C}{T\beta_T}\right)[T_1 - T(X, -L/2)] \tag{11}$$

$$\left[\frac{d^3U}{dY^3}-\frac{1}{\kappa}\frac{dU}{dY}-\frac{C_f}{\nu\sqrt{\kappa}}\frac{dU^2}{dY}\right]_{Y=L/2}=\frac{\beta_T g h_2}{k\nu}\left(1-\frac{k\beta_C}{T\beta_T}\right)[T(X,L/2)-T_2] \tag{12}$$

From the above Eq. (6) it shows that $\partial T/\partial X$ is not depending on Y-coordinate. Also from Eqs. (11) and (12), it shows that $\partial T/\partial X$ is zero for both borders. On account of Eqs. (6), there exist a constant A such as

$$\frac{dP}{dX}=A \tag{13}$$

where A is fixed and the heat transport equation is written as follows

$$\frac{d^2T}{dY^2}=-\frac{\nu}{\alpha C_p}\left(\frac{dU}{dY}\right)^2-\frac{\nu U^2}{\alpha C_P\kappa} \tag{14}$$

and the concentration equation is given as

$$\frac{d^2C}{dY^2}=-\frac{k}{T}\frac{d^2T}{dY^2} \tag{15}$$

From Eqs. (8) and (14) allow one to obtain differential equation as

$$\frac{d^4U}{dY^4}=\frac{\beta_T g}{\alpha C_p}\left(\frac{dU}{dY}\right)^2-\frac{\beta_C g k}{\alpha C_p T}\left(\frac{dU}{dY}\right)^2+\frac{1}{\kappa}\frac{d^2U}{dY^2}+\frac{\beta_T gU^2}{\alpha C_p\kappa}-\frac{\beta_C gkU^2}{\alpha C_p T\kappa}+\frac{C_f}{\nu\sqrt{\kappa}}\frac{d^2U^2}{dY^2} \tag{16}$$

The conditions for the velocity become

$$U(-L/2)=0,\quad U(L/2)=0 \tag{17}$$

along with Eqs. (11) and (12), (using Eq. (5)) can be expressed as

$$\left[\frac{d^3U}{dY^3}-\frac{1}{\kappa}\frac{dU}{dY}-\frac{h_1}{k}\frac{d^2U}{dY^2}-\frac{C_f}{\nu\sqrt{\kappa}}\frac{dU^2}{dY}\right]_{Y=-L/2}$$
$$=-\frac{Ah_1}{\mu k}-\frac{h_1U}{k\kappa}-\frac{C_fh_1U^2}{\nu k\sqrt{\kappa}}+\frac{\beta_T g h_1}{\nu k}[T_1-T_0+C_1-C_0] \tag{18}$$

$$\left[\frac{d^3U}{dY^3}-\frac{1}{\kappa}\frac{dU}{dY}+\frac{h_2}{k}\frac{d^2U}{dY^2}-\frac{C_f}{\nu\sqrt{\kappa}}\frac{dU^2}{dY}\right]_{Y=L/2}$$
$$=\frac{Ah_2}{\mu k}+\frac{h_2U}{k\kappa}+\frac{h_2C_fU^2}{\nu k\sqrt{\kappa}}+\frac{\beta_T g h_2}{\nu k}[T_0-T_2+C_2-C_0] \tag{19}$$

Using Eq. (14), Eq. (15) can be rewritten as

$$\frac{d^2C}{dY^2}=\frac{k\nu}{T\alpha C_p}\left(\frac{dU}{dY}\right)^2+\frac{k\nu U^2}{T\alpha C_p\kappa} \tag{20}$$

The concentration conditions are

$$C\left(-\frac{L}{2}\right)=C_1,\quad C\left(\frac{L}{2}\right)=C_2 \tag{21}$$

Equations (15) to (21) will explain the velocity and concentration distributions. These equations are rewritten in a non-dimensional form with the help of the non-dimensional quantities

$$u=\frac{U}{U_0},\quad \theta=\frac{T-T_0}{\Delta T},\quad y=\frac{Y}{D},\quad GR_T=\frac{g\beta_T\Delta TD^3}{\nu^2},\quad Re=\frac{U_0D}{\nu},$$
$$Br=\frac{U_0^2\mu}{k\Delta T},\quad R_T=\frac{T_2-T_1}{\Delta T},\quad GR_C=\frac{g\beta_C\Delta TD^3}{\nu^2},\quad \Lambda_1=\frac{GR_T}{Re},\quad \Lambda_2=\frac{GR_C}{Re},$$
$$Bi_1=\frac{h_1D}{k},\quad Bi_2=\frac{h_2D}{k},\quad S=\frac{Bi_1Bi_2}{Bi_1Bi_2+2Bi_1+2Bi_2},\quad U_0=-\frac{AD^2}{48\mu},$$
$$\phi=\frac{C-C_0}{\Delta C},\quad Sc=\frac{\nu}{D_m},\quad Sr=\frac{k\Delta TD_m}{T\Delta C\nu},\quad \sigma=\frac{D}{\sqrt{\kappa}},\quad I=\frac{\rho C_fD^2U_0}{\mu\sqrt{\kappa}} \tag{22}$$

The reference velocity, temperature and concentrations are

$$U_0=-\frac{AD^2}{48\mu},\quad T_0=\frac{T_1+T_2}{2}+S\left(\frac{1}{Bi_1}-\frac{1}{Bi_2}\right)[T_2-T_1],\quad C_0=\frac{C_1+C_2}{2} \tag{23}$$

The temperature drop ΔT and the reference concentration drop ΔC are

$$\Delta T=T_2-T_1 \text{ if } T_1<T_2 \tag{24}$$

$$\Delta T=\frac{\nu^2}{C_pD^2} \text{ if } T_1=T_2 \tag{25}$$

$$\Delta C=C_2-C_1 \tag{26}$$

For symmetric wall temperature the value of R_T is equal to zero and the value of R_T is equal to one for asymmetric conditions. By using the non-dimensional quantities from Eq. (22), Eqs. (16)–(21) are reloaded as

$$\frac{d^4u}{dy^4}=\sigma^2\frac{d^2u}{dy^2}+I\frac{d^2u^2}{dy^2}+(\Lambda_1-\Lambda_2SrSc)Br\left(\frac{du}{dy}\right)^2+(\Lambda_1-\Lambda_2SrSc)Br\sigma^2u^2 \tag{27}$$

with boundary conditions on velocity

$$u(-0.25)=u(0.25)=0 \tag{28}$$

$$\left[\frac{d^2u}{dy^2}-\frac{1}{Bi_1}\frac{d^3u}{dy^3}+\frac{\sigma^2}{Bi_1}\frac{du}{dy}+\frac{I}{Bi_1}\frac{du^2}{dy}-u\sigma^2-Iu^2\right]_{y=-0.25}$$
$$=-48+\frac{R_T\Lambda_1S}{2}\left(1+\frac{4}{Bi_1}\right)+\frac{\Lambda_2}{2} \tag{29}$$

$$\left[\frac{d^2u}{dy^2}+\frac{1}{Bi_2}\frac{d^3u}{dy^3}-\frac{\sigma^2}{Bi_2}\frac{du}{dy}-\frac{I}{Bi_2}\frac{du^2}{dy}-u\sigma^2-Iu^2\right]_{y=0.25}$$
$$=-48-\frac{R_T\Lambda_1S}{2}\left(1+\frac{4}{Bi_2}\right)-\frac{\Lambda_2}{2} \tag{30}$$

$$\frac{d^2\phi}{dy^2}+BrSrSc\left(\frac{du}{dy}\right)^2+BrSrSc\sigma^2u^2=0 \tag{31}$$

$$\phi(-0.25)=-0.5,\ \phi(0.25)=0.5 \tag{32}$$

Similarly Eqs. (14) and (22) yield

$$\frac{d^2\theta}{dy^2}+Br\left(\frac{du}{dy}\right)^2-\sigma^2u^2=0 \tag{33}$$

while from Eqs. (5) and (22) one obtains

$$\theta=-\frac{1}{\Lambda_1}\left(48+\frac{d^2u}{dy^2}+\Lambda_2\phi-\sigma^2u-Iu^2\right) \tag{34}$$

Method of solution

The analytical solutions for Eqs. (27)–(32) can be found for low Brinkman number owing to nonlinear nature of thee equations. The solutions of Eqs. (27)–(32) can be written using the series nature as

$$u(y)=u_0(y)+Br\cdot u_1(y)+Br^2\cdot u_2(y)+\ldots \tag{35}$$

$$\phi(y)=\phi_0(y)+Br\cdot\phi_1(y)+Br^2\cdot\phi_2(y)+\ldots \tag{36}$$

Substituting Eqs. (35) and (36) we receive the solutions for Eqs. (27)–(30). Equating the terms for $Br=0$ the following equations are resolved along with the conditions on the walls in the absence of inertial parameter

$$\frac{d^4u_0}{dy^4}=\sigma^2\frac{d^2u_0}{dy^2} \tag{37}$$

also the velocity boundary conditions are

$$u_0(-0.25) = u_0(0.25) = 0 \tag{38}$$

$$\left[\frac{d^2u_0}{dy^2} - \frac{1}{Bi_1}\frac{d^3u_0}{dy^3} + \frac{\sigma^2}{Bi_1}\frac{du_0}{dy} - \sigma^2 u_0\right]_{y=-0.25} = -48 + \frac{R_T\Lambda_1 S}{2}\left(1 + \frac{4}{Bi_1}\right) + \frac{\Lambda_2}{2} \tag{39}$$

$$\left[\frac{d^2u_0}{dy^2} + \frac{1}{Bi_2}\frac{d^3u_0}{dy^3} - \frac{\sigma^2}{Bi_2}\frac{du_0}{dy} - \sigma^2 u_0\right]_{y=0.25} = -48 - \frac{R_T\Lambda_1 S}{2}\left(1 + \frac{4}{Bi_2}\right) - \frac{\Lambda_2}{2} \tag{40}$$

Equation (37) when solved become

$$u_0(y) = C_1 + C_2 y + C_3 \cdot \sinh(\sigma y) + C_4 \cdot \cosh(\sigma y) \tag{41}$$

Comparing the coefficients of first order of *Br*, the equations reduced are

$$\frac{d^4u_1}{dy^4} - \sigma^2\frac{d^2u_1}{dy^2} = (\Lambda_1 - \Lambda_2 ScSr)\left[\left(\frac{du_0}{dy}\right)^2 + \sigma^2 u_0^2\right] \tag{42}$$

with the boundary conditions

$$u_1(-0.25) = u_1(0.25) = 0 \tag{43}$$

$$\left[\frac{d^2u_1}{dy^2} - \frac{1}{Bi_1}\frac{d^3u_1}{dy^3} + \frac{\sigma^2}{Bi_1}\frac{du_1}{dy} - \sigma^2 u_1\right]_{y=-0.25} = 0 \tag{44}$$

$$\left[\frac{d^2u_1}{dy^2} + \frac{1}{Bi_2}\frac{d^3u_1}{dy^3} - \frac{\sigma^2}{Bi_2}\frac{du_1}{dy} - \sigma^2 u_1\right]_{y=0.25} = 0 \tag{45}$$

Using Eq. (36) in Eq. (31) and equating parameters of $Br = 0$, the following differential equation is obtained

$$\frac{d^2\phi_0}{dy^2} = 0 \tag{46}$$

with the boundary conditions

$$\phi_0(-0.25) = -0.5,\ \phi_0(0.25) = 0.5 \tag{47}$$

The solution of Eq. (46) is given by

$$\phi_0 = C_5 y + C_6 \tag{48}$$

Similarly collecting the coefficient of first order of *Br*, the reduced equation is

$$\frac{d^2\phi_1}{dy^2} = -Sc \cdot Sr\left[\left(\frac{du_0}{dy}\right)^2 + \sigma^2 u_0^2\right] \tag{49}$$

with the boundary conditions

$$\phi_1(-0.25) = \phi_1(0.25) = 0 \tag{50}$$

Overall heat, mass and momentum transport parameters

The Nusselt number, wall friction and Sherwood number in non-dimensional view can be shown as

$$Nu_1 = \frac{D}{R_T[\theta(0.25) - \theta(-0.25)] + (1 - R_T)}\left.\frac{d\theta}{dy}\right|_{y=-0.25} \tag{51}$$

$$Nu_2 = \frac{D}{R_T[\theta(0.25) - \theta(-0.25)] + (1 - R_T)}\left.\frac{d\theta}{dy}\right|_{y=0.25} \tag{52}$$

$$\tau_1 = \left(\frac{du}{dy}\right)_{y=-0.25},\ \tau_2 = \left(\frac{du}{dy}\right)_{y=0.25} \tag{53}$$

$$Sh_1 = \left(\frac{d\phi}{dy}\right)_{y=-0.25},\ Sh_2 = \left(\frac{d\phi}{dy}\right)_{y=0.25} \tag{54}$$

The exact solution of Eq. (27) can not be computed as the equation is nonlinear. Therefore the approximate solution is procured computationally employing Runge–Kutta technique with the suitable shooting scheme. The solutions are validated for *Br* taken while evaluating the perturbation solutions as shown in Table 1.

Results and discussion

In this part, the outcomes on the double diffusion of permeable fluid embedded in a vertical tube are presented. Opting similar and dissimilar temperatures on the plates for same and different Biot numbers, the consequence of thermal and mass numbers, Schmidt, Soret, Brinkman numbers, inertia parameter and Darcy number are evaluated and detailed in Figs. 2 to 10. Neglecting inertia effects ($I = 0$), viscous dissipation ($Br = 0$) and buoyancy forces ($\Lambda_1 = 0$), the exact solutions are found and the plots are demonstrated in Fig. 2. The velocity curve is parabolic for $\sigma = 2, 8$ and $\Lambda_1 = 0$. Flow reversal appears at the left border ($\Lambda_1 = 1000$) and at the right border ($\Lambda_1 = -1000$) which is the similar remark made by Gebhart et al. [52] for pure viscous fluid using isothermal boundary settings.

The impact of Brinkman and Darcy numbers for forced convection can be seen in Figs. 3a and 3b for equal and distinct *Bi*. The temperature curve is linear when $Br = 0$ for $\sigma = 2$ and also for $\sigma = 8$ due to conduction heat transfer. The energy is elevated for larger values of *Br* for same and different *Bi*. However, the behavior of temperature profiles for $Bi_1 = Bi_2$ and $Bi_1 \neq Bi_2$ are not the same. The temperature escalates from left surface to the right surface when $Bi_1 = Bi_2$ and decreases from left surface to the right surface for diverse Biot numbers. For values of $Br \neq 0$, the heat transfer is dominated by convective energy transport in the boundary layer. Further the value of $S = 0.61$ for $Bi_1 = Bi_2$ and $S = 0.25$ for $Bi_1 \neq Bi_2$ which influence the temperature filed at the boundaries. Figs. 3a and 3b also infer that as σ boosts, the temperature is reduced.

Table 1
Values of skin friction.

	$Bi_1 = Bi_2 = 10$		$Bi_1 = 1.0, Bi_2 = 10$	
τ1	τ1	τ_2	τ1	τ_2
Λ_1				
0	8.87178725	−9.28222622	8.89183867	−9.28226638
10	8.88286395	−9.83583325	9.52673318	−9.95143360
15	8.89210416	−10.1286269	9.94700492	−10.3599839
20	8.91244460	−10.4341781	10.4753474	−10.8458322
Λ_2				
0	9.07877372	−9.35833836	9.37954484	−9.40235447
10	8.68764082	−9.75001774	8.98386536	−9.79152915
15	8.49215286	−9.94593623	8.78625833	−9.98627924
20	8.29671723	−10.1419072	8.5888067	−10.1811381
Br				
0	8.75230559	−9.42160378	8.83074396	−9.34317474
0.01	8.76502450	−9.43448594	8.86366860	−9.36701123
0.1	8.88318115	−9.55415192	9.18162758	−9.59688762
0.5	9.51222837	−10.1909653	11.5100612	−11.2709386
Sr				
0.5	8.88318115	−9.55415192	9.18162758	−9.59688762
1.0	8.88322081	−9.55420713	9.18173968	−9.59699996
1.5	8.88326048	−9.55426241	9.18185178	−9.59711231
2.0	8.88330016	−9.55431770	9.18196391	−9.59722468
Sc				
0.5	8.88316131	−9.55412426	9.18157154	−9.59683146
1.0	8.88318115	−9.55415192	9.18162758	−9.59688762
1.5	8.88320100	−9.55417964	9.18168363	−9.59694379
2.0	8.88322081	−9.55420713	9.18173968	−9.59699996
I				
0.0	8.93857587	−9.61108444	9.24343091	−9.65788871
2.0	8.72763824	−9.39420513	9.00893881	−9.42624727
4.0	8.54143206	−9.20255512	8.80373377	−9.22310098
6.0	8.37498892	−9.03108048	8.62159034	−9.04243690
σ				
2.0	10.8227474	−11.5252093	11.2353465	−11.6412627
4.0	8.88318115	−9.55415192	9.18162758	−9.59688762
6.0	6.98702701	−7.61334903	7.19277728	−7.60508193
8.0	5.53484077	−6.11104002	5.68199152	−6.07819370

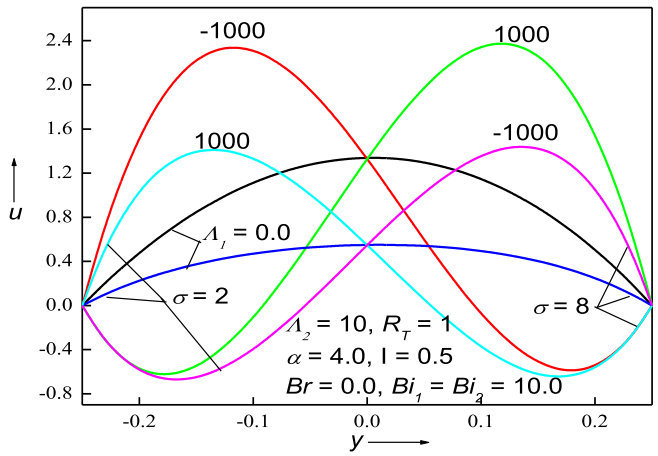

Fig. 2. Contours of velocity for various Λ_1.

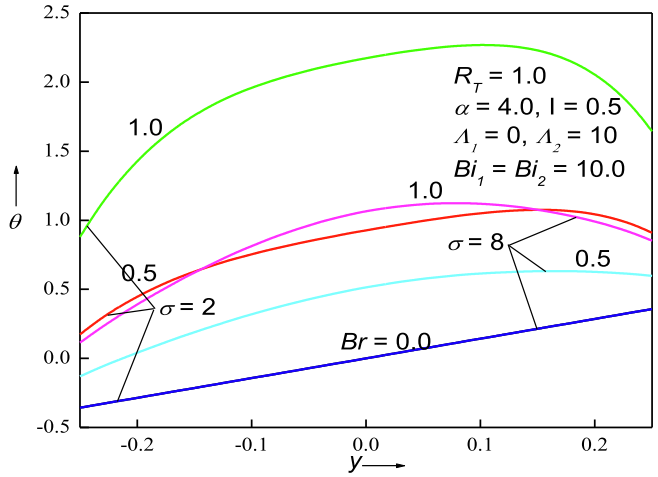

Fig. 3a. Contours of temperature for various *Br*.

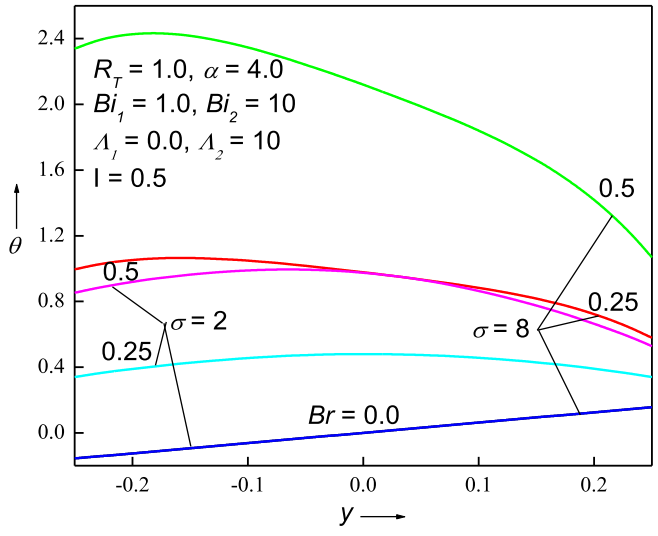

Fig. 3b. Contours of temperature for various *Br*.

The Darcy number is the inverse of permeability, therefore developing the Darcy number implies that the permeability is decreased which results in the gain of the resistance of solid matrix to the flow. The present results agree with Zanchini [53] in the absence of σ and concentration

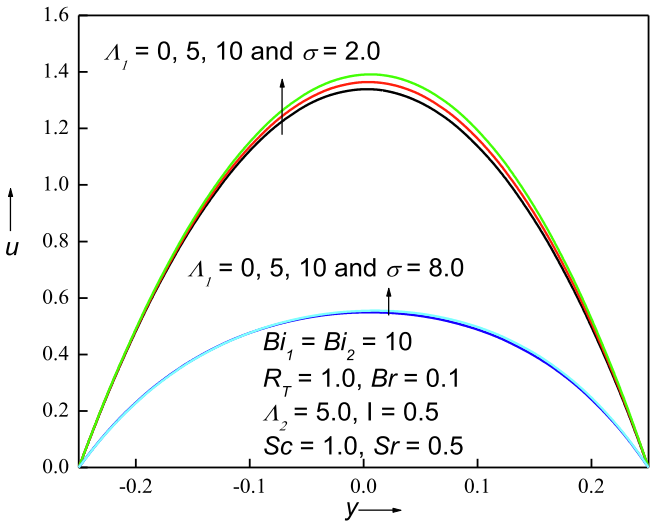

Fig. 4a. Contours of velocity for various Λ_1.

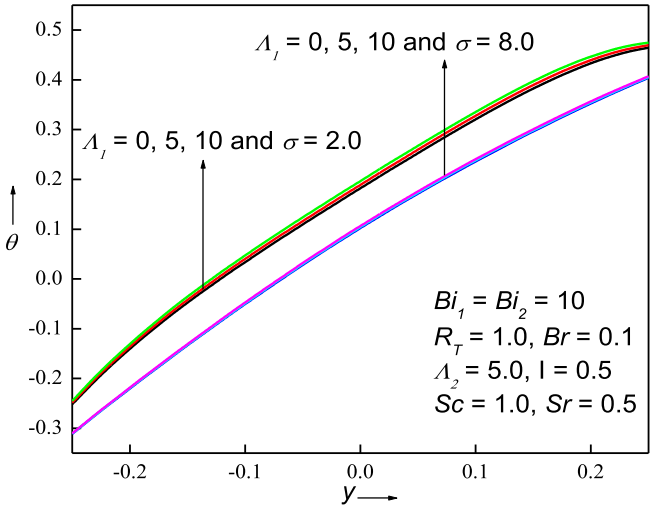

Fig. 4b. Contours of temperature for various Λ_1.

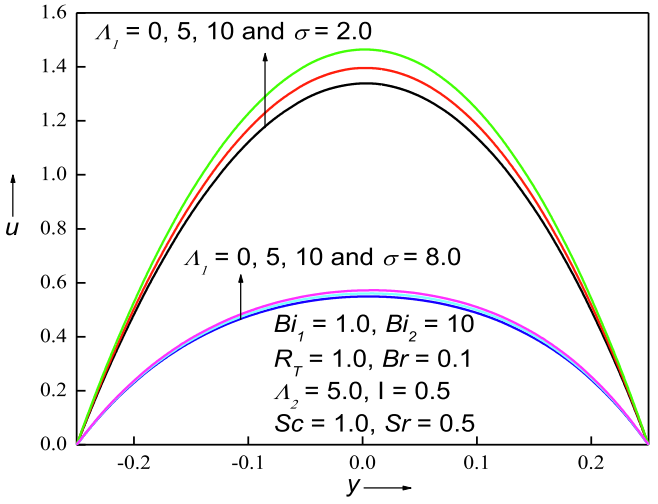

Fig. 4c. Contours of velocity for various Λ_1.

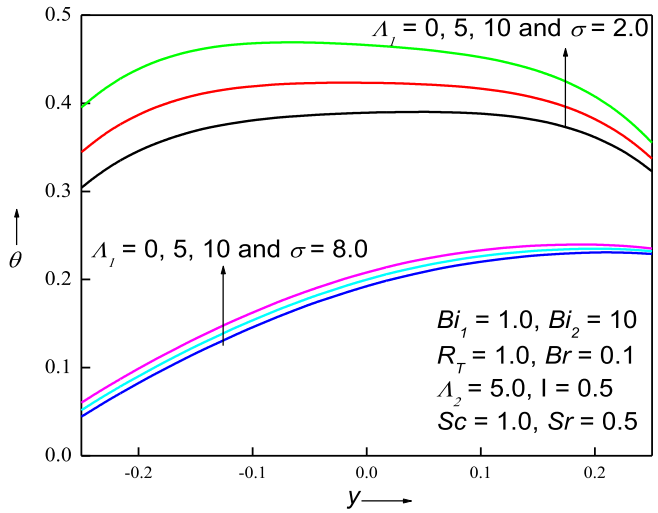

Fig. 4d. Contours of temperature for various Λ_1.

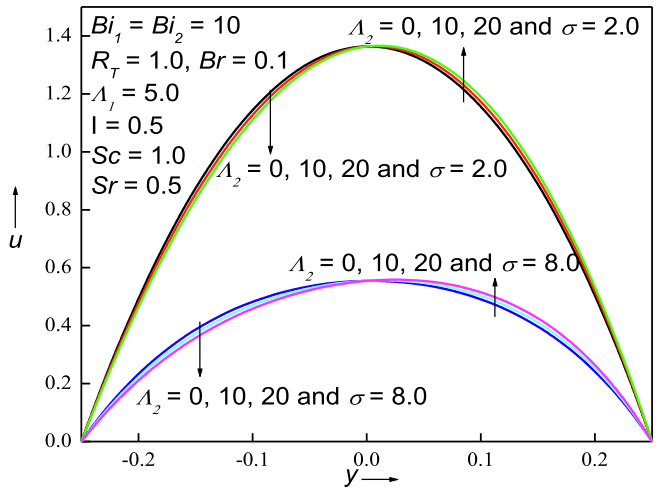

Fig. 5. Contours of velocity for various Λ_2.

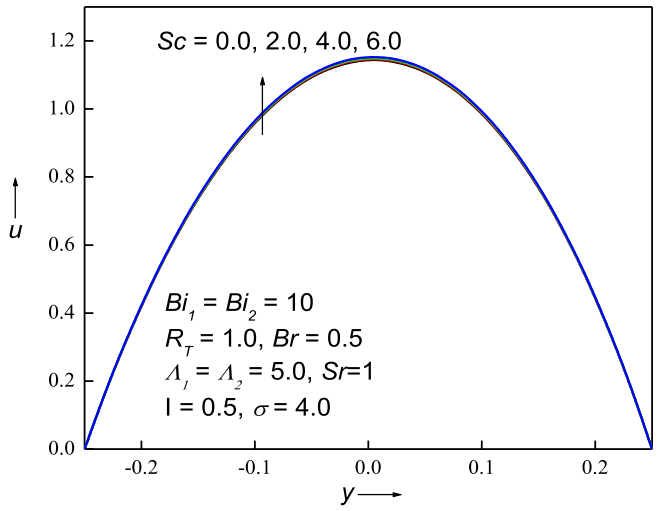

Fig. 6a. Contours of velocity for various Sc.

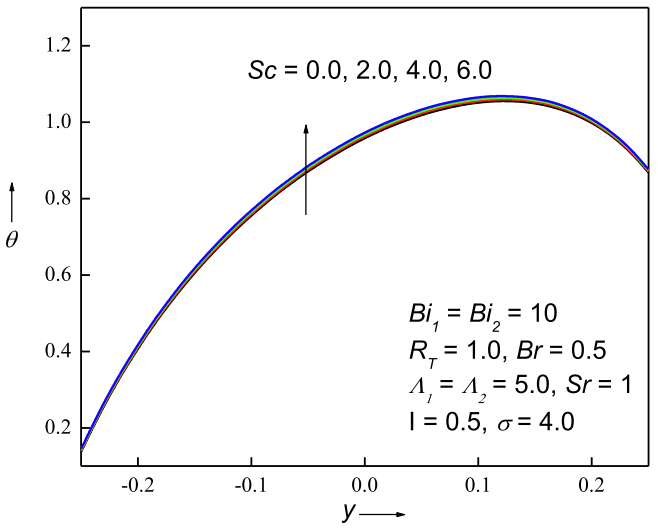

Fig. 6b. Contours of temperature for various Sc.

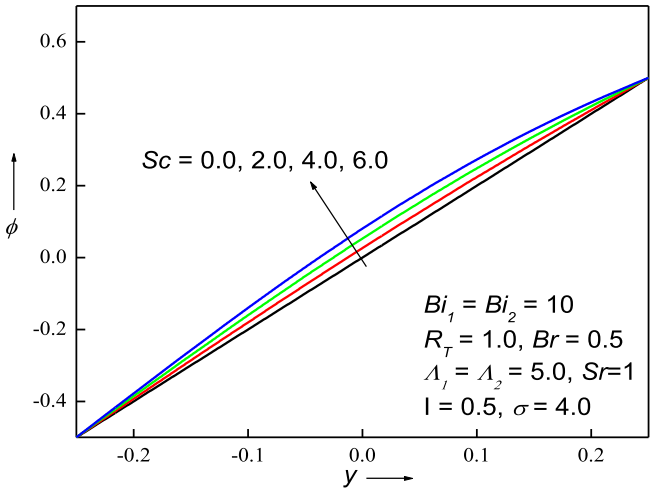

Fig. 6c. Contours of concentration for various Sc.

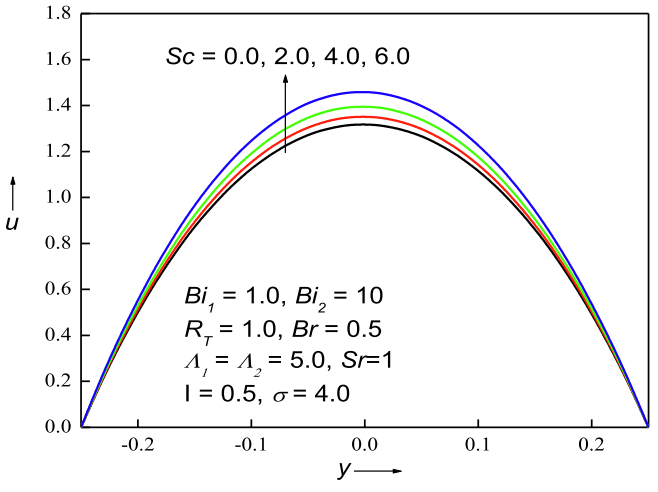

Fig. 6d. Contours of velocity for various Sc.

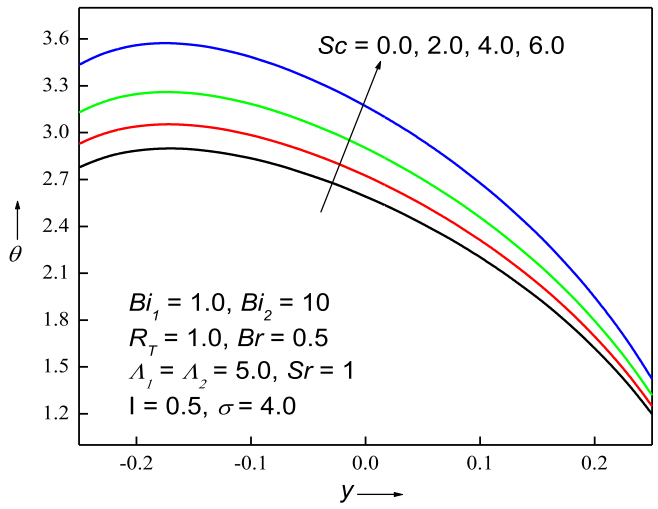

Fig. 6e. Contours of temperature for various *Sc*.

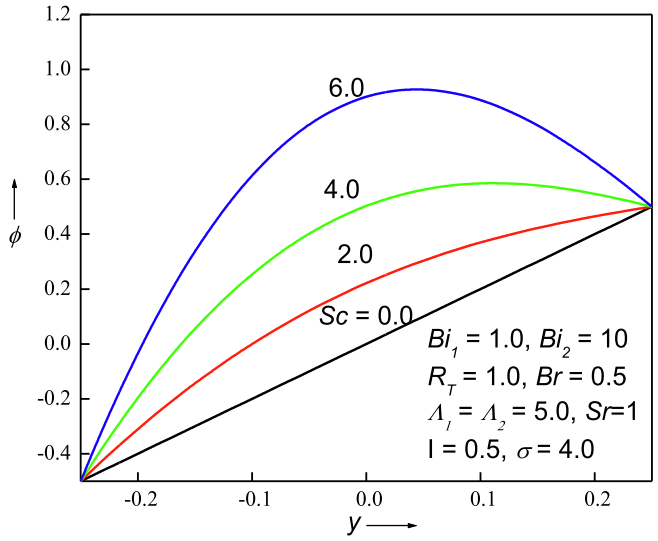

Fig. 6f. Contours of concentration for various *Sc*.

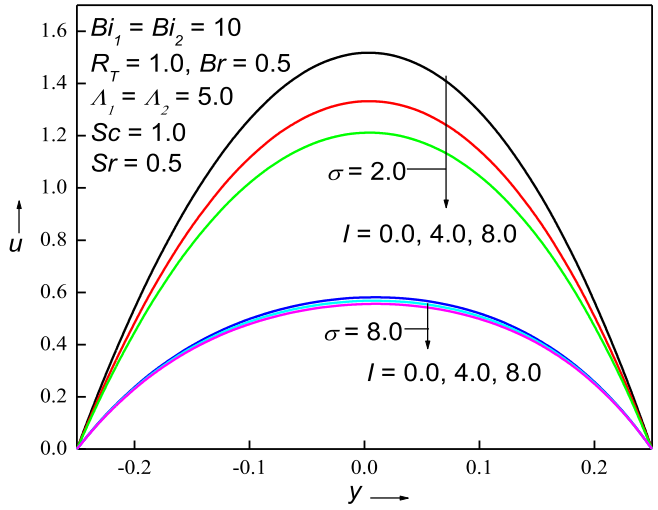

Fig. 7a. Contours of velocity for various *I*.

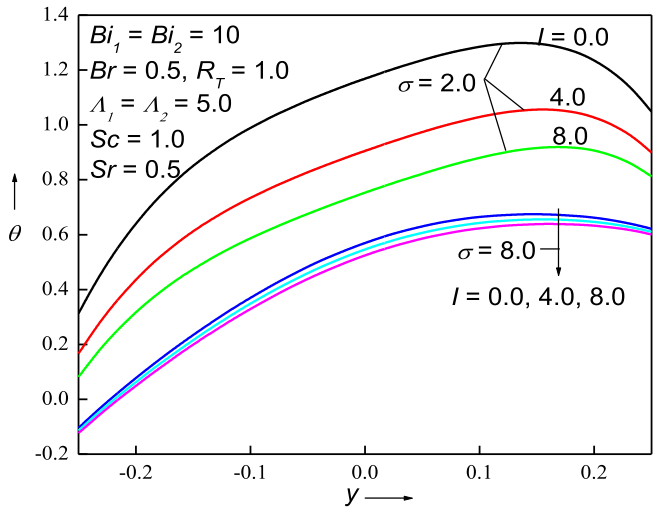

Fig. 7b. Contours of temperature for various *I*.

Grashof number.

Figs. 4a to 4d design the outcome of Λ_1 and σ for same and different *Bi*. Increasing the modified heat Grashof number enhances the both the momentum and thermal fields for uniform and non-uniform Biot numbers. As seen in Eq. (27), the terms $\Lambda_1 \left(\frac{du}{dy}\right)^2$ and $\Lambda_1 \cdot u^2$ imply that increasing Λ_1 results in enhancing the momentum as there is an augmentation of the buoyancy. Increment of the velocity field also rises the temperature field (Eq. (33)) owing to the increase in viscous dissipation. The nature of velocity profiles for $Bi_1 = Bi_2$ (Fig. 4a) and $Bi_1 \neq Bi_2$ (Fig. 4b) are similar whereas the temperature profiles are different (Fig. 4b and 4d). The effect of Λ_1 is more operative for $Bi_1 \neq Bi_2$ when compared with $Bi_1 = Bi_2$. The Darcy parameter diminishes the circulation field for both $Bi_1 = Bi_2$ and $Bi_1 \neq Bi_2$ owing to the evidence that the Darcian and inertial drag suppress the convection.

The effect of concentration Grashof number Λ_2 and σ on the velocity pattern is displayed in Fig. 5 for equal Biot numbers. As Λ_2 increases velocity reduces on the left border and rises on the right border for σ = 2 and 8. Physically increase in Λ_2 implies the increase in species buoyancy force. However the effect of Λ_2 is not very influential. The influence of Λ_2 on the velocity for various *Bi* shows the similar impact as that of equal *Bi* and hence not shown pictorially. The effect of Λ_2 on the temperature field for $Bi_1 = Bi_2$ and $Bi_1 \neq Bi_2$ shows the similar effects as that Λ_1 (Figs. 4a and 4d) and hence not presented graphically. The influence of Schmidt number *Sc* on the flow structure for same and different Biot numbers is plotted in Figs. 6a to 6f. The influence of *Sc* is to promote the velocity, temperature and concentration patterns. The magnitude of promotion is predominant on the velocity and concentration distributions for different *Bi* compared with equal *Bi*. The magnitude of temperature is less at the cold plate when compared with the hot plate for $Bi_1 = Bi_2$ and the effect of *Sc* is not very influential (Fig. 6b). For $Bi_1 \neq Bi_2$ the temperature at the cold plate is very high compared to the hot wall and the effect of *Sc* is very much influential on the temperature (Fig. 6e). The effect of *Sc* on the concentration field is symmetric and is more operative for $Bi_1 \neq Bi_2$ (Fig. 6f) when compared with $Bi_1 = Bi_2$ (Fig. 6d).

The effect of Forchheimer inertia parameter *I* and the Darcy number σ on the velocity and temperature patterns is demonstrated in Figs. 7a and 7b. The velocity profiles are parabolic for equal *Bi* (Fig. 7a) and the profiles are reduced with a rise of *I* and σ. One can also view that inertial parameter is more operative for σ = 2 when compared with σ = 8 (similar results as pointed out by Lai and Kulacki [54]. Similar effect is observed for various *Bi* and hence not figured. The effects of *I* and σ on the temperature are shown in Fig. 7b which reflects that the fluid becomes cold as *I* and σ increase and the magnitude is less at the cold plate

compared with the hot plate for $Bi_1 = Bi_2$. The effect of I and σ for $Bi_1 \neq Bi_2$ is the similar outcomes for the influence of Λ_1 (Fig. 4d) and hence not displayed graphically. The impacts of Br and porous characteristic on the evaluation of velocity and temperature show similar nature as that of Λ_1 (Figs. 4a to 4d) and hence dropped the pictorial presentation. The impact of Br enhances the flow for any values of Bi and σ. However the unequal Bi cause higher values of temperature compared to equal Bi.

Wall friction, Nu and Sh are calculated for all the pertinent parameters and tabulated in Tables 1–3, respectively. The values tabulated infer that the skin friction is elevated in magnitude at both the plates with Λ_1, Br, Sr, Sc whereas it is diminished with inertial and porous characteristics for same and various Bi. The wall friction decreases at the cold plate and increases at the hot plate in magnitude for the effects of Λ_2 for both $Bi_1 = Bi_2$ and $Bi_1 \neq Bi_2$ as shown in Table 1. The Nusselt number increases at the cold plate and decreases at the hot plate for promoting the values for Λ_1 and Br whereas the reversal effect is obtained for the effects of I and σ but it decreases at both the plates by promoting Λ_2 when $Bi_1 = Bi_2$. For unequal Biot numbers, Nu rises on the left border for the effects of Λ_1 and Br whereas it decreases with the parameters Λ_2, I and σ. At the right plate it increases in magnitude by operating Λ_1 and Λ_2, and decreases with Br, I and σ. The rate of heat transfer does not replicate significant change for the effects of Soret and Schmidt numbers as tabulated in Table 2.

Table 3 reflects the nature of Sherwood number and it summarizes that it is augmented at the left border and degraded on the right surface for the changes in Λ_1, Λ_2, Br, Sr and Sc, reversal effect is seen for the effects of I and σ when Biot numbers are taken to be equal. For different Biot numbers, the Sherwood number at the left plate increases with Λ_1, Λ_2, Br, I and σ whereas it decreases with Sr and Sc in magnitude. At the hot wall it is reduced with Λ_1, Br, I, σ and increased with Λ_2, Sr and Sc. The parameters are chosen as $\Lambda_1 = \Lambda_2 = 5.0$, $R_T = 1.0$, $Br = 0.1$, $Sc = 1.0$, $Sr = 0.5$, $I = 0.5$, σ = 4.0 for evaluating the values in all the tables except the varying one.

Table 2
Values of Nusselt numbers

$Bi_1 = Bi_2 = 10$			$Bi_1 = 1.0$, $Bi_2 = 10$	
	Nu_1	Nu_2	Nu_1	Nu_2
Λ_1				
0	2.26437423	0.57451333	0.99066865	−0.69921433
10	2.30754945	0.50363670	1.04717256	−0.90407044
15	2.33287154	0.46363310	1.08555439	−1.04145840
20	2.36122838	0.41995316	1.13510863	−1.21719883
Λ_2				
0	2.29361750	0.55025586	1.02045619	−0.78844636
10	2.27645374	0.53026100	1.01225799	−0.79710256
15	2.26848104	0.51965314	1.00843964	−0.80242140
20	2.26091404	0.50863791	1.00480814	−0.80840077
Br				
0	1.42857143	1.42857143	0.62500000	0.62500000
0.01	1.51179348	1.34221464	0.66169474	0.49158647
0.1	2.28483260	0.54046192	1.01626343	−0.79244423
0.5	6.37931828	−3.69490325	3.59294356	−9.90400625
Sr				
0.5	2.28483260	0.54046192	1.01626343	−0.79244423
1.0	2.28484300	0.54045016	1.01627525	−0.79248680
1.5	2.28485344	0.54043844	1.01628707	−0.79252937
2.0	2.28486388	0.54042671	1.01629889	−0.79257196
Sc				
0.5	2.28482740	0.54046779	1.01625752	−0.79242294
1.0	2.28483260	0.54046192	1.01626343	−0.79244423
1.5	2.28483789	0.54045611	1.01626934	−0.79246551
2.0	2.28484300	0.54045016	1.01627525	−0.79248680
I				
0.0	2.29935010	0.52560281	1.02328893	−0.81767493
2.0	2.24477679	0.58147352	0.99698079	−0.72317487
4.0	2.19819688	0.62919112	0.97473450	−0.64322199
6.0	2.15782548	0.67057308	0.95559660	−0.57440681
σ				
2.0	2.51293026	0.30610072	1.12568041	−1.18568658
4.0	2.28483260	0.54046192	1.01626343	−0.79244423
6.0	2.06128363	0.77041854	0.91121782	−0.41418055
8.0	1.89191422	0.94499086	0.83304279	−0.13206230

Table 3
Values of Sherwood numbers

$Bi_1 = Bi_2 = 10$			$Bi_1 = 1.0$, $Bi_2 = 10$	
	Sh_1	Sh_2	Sh_1	Sh_2
Λ_1				
0	2.21749822	1.70848061	3.51798930	0.98784394
1	2.24984602	1.67061018	4.10994688	0.61039489
5	2.54050996	1.34070829	−6.22444481	−11.7264946
10	−0.53287711	−2.59845293	2.25417611	0.40579230
Λ_2				
0	2.52116343	1.36723045	2.04368743	−2.30513244
1	2.52481004	1.36219162	−0.15852739	−3.81672866
5	2.54050996	1.34070829	−6.22444481	−11.7264946
10	2.56300501	1.31043751	−1.24259331	−6.47981796
Br				
0.0	2.00000000	2.00000000	2.00000000	2.00000000
0.01	2.00004989	1.99994298	2.00000644	1.99998668
0.1	2.00043102	1.99883100	2.00124589	1.99859278
0.5	2.03570043	1.94239353	2.46527912	1.68788265
Sr				
0.5	2.54050996	1.34070829	−6.22444481	−11.7264946
1.0	3.12718273	0.63020006	−5.88796949	−13.9919850
1.5	3.76928703	−0.14162993	−4.38387615	−16.6073931
2.0	4.47940296	−0.98847164	−4.24946989	−17.5973595
Sc				
0.5	2.26496784	1.67622877	−6.24328914	−9.91782194
1.0	2.54050996	1.34070829	−6.22444481	−11.7264946
1.5	2.82755882	0.99242050	−5.45238718	−12.9497405
2.0	3.12718273	0.63020006	−5.88796949	−13.9919850
I				
0.0	2.58180340	1.29499778	−6.14646629	−12.2930895
2.0	2.44426092	1.44792527	−3.18197792	−10.6625211
4.0	2.35656141	1.54666087	1.26751431	−9.87162384
6.0	2.29562665	1.61605619	6.53716875	−8.37194710
σ				
2.0	2.98197286	0.85106290	−11.0253776	−15.9857445
4.0	2.54050996	1.34070829	−6.22444481	−11.7264946
6.0	2.25608168	1.66466167	0.95280553	−4.38768348
8.0	2.12159846	1.82455884	1.49062305	1.25702190

The numerical values obtained in the graphs and tables are evaluated using Runge-Kutta algorithm with shooting technique. These solutions are further justified by solving the governing equations using regular perturbation technique. Brinkman number is employed to act as the perturbation characteristic. The solution of first order (u_1) is obtained using the software MATHEMATICA and the total solution $u = u_0 + Br\, u_1$ is tabulated in Table 4. Without viscous dissipation effects, the analytical and numerical values are equal. The difference between numerical and regular perturbation method is enhanced as Brinkman number increases. This is a valid notification as the regular perturbation method should be used for low perturbation characteristic. It is also identified that the difference increases in a large magnitude on the temperature for different Biot numbers in comparison with same Bi.

Conclusions

Chemically reacting fluid embedded in a vertical duct saturated with porous matrix was studied employing the Robin border restrictions. Non-Darcy model including the Forchheimer drag effect was employed to define the porous medium influence. The heat and mass balance equations were decoded with the momentum equation resulting in solving fourth order nonlinear momentum equation. This equation was solved completely opting Runge-Kutta-shooting method which was a numerical scheme and also regular perturbation technique (valid only for low Br and in the absence of inertial force). The computations portrayed the following

Table 4
Values of velocity $u = u_0 + Br\, u_1$

y	$Bi_1 = Bi_2 = 10$					
	$Br = 0$		$Br = 0.01$		$Br = 0.5$	
	Analytical	Numerical	Analytical	Numerical	Analytical	Numerical
−0.25	0.00000000	0.00000000	0.00000000	0.00000000	0.00000000	0.00000000
−0.15	0.67965726	0.67965726	0.68021767	0.68073003	0.707677973	0.74418300
−0.05	1.00914212	1.00914212	1.00997170	1.01076494	1.050621450	1.10679409
0.05	1.02450616	1.02450616	1.02533845	1.02613307	1.066120815	1.12240376
0.15	0.71086793	0.71086793	0.71143405	0.71194906	0.739173772	0.77588913
0.25	0.00000000	0.00000000	0.00000000	0.00000000	0.00000000	0.00000000
y	$Bi_1 = 1.0$, $Bi_2 = 10$					
	$Br = 0$		$Br = 0.01$		$Br = 0.5$	
	Analytical	Numerical	Analytical	Numerical	Analytical	Numerical
−0.25	0.00000000	0.00000000	0.00000000	0.00000000	0.00000000	0.00000000
−0.15	0.68331476	0.68331476	0.684892468	0.68582544	0.76220016	0.89254566
−0.05	1.01094259	1.01094259	1.013109122	1.01445576	1.11926914	1.30374964
0.05	1.02270569	1.02270569	1.024721891	1.02600708	1.12351597	1.29753233
0.15	0.70721043	0.70721043	0.708482925	0.70929094	0.770835053	0.87995753
0.25	0.000000000	0.00000000	0.00000000	0.00000000	0.00000000	0.00000000

1. The numerical and analytical solutions were in good agreement for low *Br* and the present solutions have a good agreement with Zanchini Zanchini [53] without Λ_2.
2. Flow reversal appears at the hot wall for buoyancy opposing motion and at the cold wall for buoyancy assisting motion without dissipation. Rising viscous dissipation accelerates the fluid flow for negligible buoyancy forces.
3. Embracing the buoyancy forces and dissipations, the thermal Grashof number augments the flow for symmetric and asymmetric Biot numbers. The velocity, temperature and concentration fields were gained with the enlargement of Schmidt and Soret parameters. Second order Forchheimer inertial parameter and Darcy number assault the flow depletion.
4. The wall friction was boosted with the step-up of Λ_1, *Br*, *Sr* and *Sc* while it was declined with inertial and porous characteristic. The strength of energy transport was upswing with Λ_1 and *Br* while it was shrinked with the inertial and porous parameter. The Sherwood number was enhanced at the left plate and declined at the right plate for the blowing up Λ_1 and Λ_2, *Br*, *Sr* and *Sc* while it was depressed with the inertial and porous parameters.

CRediT authorship contribution statement

J.C. Umavathi: Conceptualization, Methodology, Data curation, Writing - original draft, Writing - review & editing. **Bernardo Buonomo:** Methodology, Writing - review & editing. **Oronzio Manca:** Methodology, Writing - review & editing. **Mikhail A. Sheremet:** Methodology, Writing - review & editing.

Declaration of Competing Interest

The authors declare that they have no known competing financial interests or personal relationships that could have appeared to influence the work reported in this paper.

References

[1] Darcy, H. P. G., Les Fontaines Publiques de la ville de Dijon, Paris, Vector Dalmont, 1856.
[2] A. Nakayama, T. Kokudai, H. Koyama, Non-Darcian boundary layer flow and forced convective heat transfer over a flat plate in a fluid-saturated porous medium, ASME J. Heat Transfer 112 (1990) 157–162.
[3] H.C. Brinkman, On the permeability of media consisting of closely packed porous Particles, Appl. Sci. Res. A 1 (1975) 81–86.
[4] Forchheimer, P, Wasserbewegung durch Boden, Z. Ver. Deut, Ing, 1901, 45, pp. 1736-1741.
[5] A.V. Kuznetsov, M. Xiong, D.A. Nield, Analytical Study of fluid flow and heat transfer during forced convection in a composite channel partially filled with a Brinkman-Forchheimer porous medium, Flow, Turbulence and Combustion 60 (1998) 173–192.
[6] Bear, J., Dynamics of Fluids in Porous Media, New York, Elsevier, 1972.
[7] Muskat, M., The Flow of Homogeneous Fluids through Porous Media, Ann Arbor, Edwards, 1946.
[8] J.C. Umavathi, B. Mallikarjun Patil, I. Pop, On laminar mixed convection flow in a vertical porous stratum with wall heating conditions, Int. J. Transp. Phenom. 8 (2006) 127–140.
[9] J.C. Umavathi, A.J. Chamkha, M. Abdul, A. Al-Mudhaf, Oscillatory flow and heat transfer in a horizontal composite porous medium channel, Int. J. Heat Technology 25 (2006) 75–86.
[10] J.C. Umavathi, I.C. Liu, J. Prathap Kumar, D. Shaik Meera, Unsteady flow heat transfer of porous media sandwiched between viscous fluids, Appl. Math. Mech. 31 (2010) 1497–1516.
[11] M.S. Malashetty, J.C. Umavathi, J.P. Kumar, Convective flow and heat transfer in an inclined composite porous medium, J. Porous Media 4 (1) (2001) 8, https://doi.org/10.1615/JPorMedia.v4.i110.1615/JPorMedia.v4.i1.20.
[12] M.S. Malashetty, J.C. Umavathi, J. Prathap Kumar, Flow and heat transfer in an inclined channel a fluid layer sandwiched between two porous layers, J. Porous Media 8 (2005) 443–453.
[13] J. Prathap Kumar, J.C. Umavathi, M.B. Biradar, Fully developed mixed convection flow in a vertical channel containing porous and fluid layers with isothermal or isoflux boundaries, Transport in Porous Media 80 (2009) 117–135.
[14] M. Yahya, M.Z. Saghir, Thermal analysis of flow in a porous flat tube in the presence of a nanofluid: Numerical approach, Int. J. Thermofluids 10 (2021) 100095, https://doi.org/10.1016/j.ijft.2021.100095.
[15] Z. Alhajaj, A.M. Bayomy, M.Z. Saghir, M.M. Rahman, Flow of nanofluid and hybrid fluid in porous channels: Experimental and numerical approach, Int. J. Thermofluids 1-2 (2020) 100016, https://doi.org/10.1016/j.ijft.2020.100016.
[16] R.M.L. Coelho, A. Silva Telles, Extended Graetz problem accompanied by Dufour and Soret effects, Int. J. Heat and Mass Transfer 45 (15) (2002) 3101–3110.
[17] O.A. Bég, A.Y. Bakier, V.R. Prasad, Numerical study of free convection Magnetohydrodynamic heat and mass transfer from a stretching surface to a saturated porous Medium with Soret and Dufour effects, Computational Materials Science 46 (1) (2009) 57–65.
[18] Z. Luo, H. Xu, Numerical simulation of heat and mass transfer through microporous media with Lattice Boltzmann method, Thermal Science and Engineering Progress 9 (2019) 44–51.
[19] U.S. Mahabaleshwar, K.R. Nagaraju, P.N. Vinay, M.N. Nadagoud, R. Bennacer, M. A. Sheremet, Effects of Dufour and Soret mechanisms on MHD mied convective-radiative non-Newtonian liquid flow and heat transfer over a porous sheet, Thermal Science and Engineering Progress 16 (2020), 100459.
[20] N. Gajjela, M. Garvandha, The influence of magnetized couple stress heat, and mass transfer flow in a stretching cylinder with convective boundary condition, cross-diffusion, and chemical reaction, Thermal Science and Engineering Progress 18 (2020) 100517, https://doi.org/10.1016/j.tsep.2020.100517.
[21] B. Ali, Y. Nie, S. Hussain, A. Manan, M.T. Sadiq, Unsteady magneto-hydrodynamic transport of rotating Maxwell nanofluid flow on a stretching sheet with Cattaneo-Christov double diffusion and activation energy, Thermal Science and Engineering Progress 20 (2020) 100720, https://doi.org/10.1016/j.tsep.2020.100720.
[22] O. Wang, K. Wang, P. Li, Forced convective heat and mass transfer in a bidisperse porous parallel plate channel with first order reaction on the wall, Thermal Science and Engineering Progress 13 (2019), 100369.
[23] J.C. Umavathi, M.A. Sheremet, B. Buonomo, O. Manca, Convection in a vertical duct under the chemical reaction influence using Robin boundary conditions, Thermal Science and Engineering Progress 15 (2020) 100440, https://doi.org/10.1016/j.tsep.2019.100440.
[24] M.K. Partha, P.V.S.N. Murthy, G.P. Raja Sekhar, Soret and Dufour effects in a non-Darcy porous medium, *ASME*, J. Heat Transfer 128 (2006) 605–615.
[25] M. Abd El-Aziz, Thermal-diffusion and diffusion-thermo effects on combined heat and mass transfer by hydromagnetic three-dimensional free convection over a permeable stretching surface with radiation, Physics Letters A. 372 (3) (2008) 263–272.

[26] D.F. Fairbanks, C.R. Wike, Diffusion and chemical reaction in an isothermal laminar flow along a soluble flat plate, Ind. Eng. Chem. Res. 42 (1950) 471–475.
[27] U.N. Das, R. Deka, V.M. Soundalgekar, Effects of mass transfer on flow past an impulsive started infinite vertical plate with constant heat flux and chemical reaction, Forschung Im Ingenieurwesen-Engineering Research 60 (1994) 284–287.
[28] H.I. Andersson, O.R. Hansen, B. Holmedal, Diffusion of a chemically reactive species from a stretching sheet, Int. J. Heat Mass Transfer 37 (4) (1994) 659–664.
[29] J.C. Umavathi, M.A. Sheremet, Onset of double-diffusive convection of a sparsely packed Microplar fluid in a porous medium layer saturated with a nanofluid, Microfluidics and Nanofluidics 21 (2017) 121–128.
[30] J.C. Umavathi, M.B. Mohite, Double diffusive convective transport in a nanofluid saturated porous layer with cross diffusion and variation of viscosity and conductivity, Heat Transfer Asian Research 43 (7) (2014) 628–652.
[31] Umavathi, J.C. and Sasso, M., Double diffusive convection in a porous medium layer saturated with an Oldroyed nanofluid, France Conference Proceedings AIP publishers., 2017b, DOI: 10.1063/1.4972758, pp. 0201661-02016610, 2017b.
[32] J.C. Umavathi, M.A. Sheremet, O. Ojjela, G.J. Reddy, The onset of double-diffusive convection in a nanofluid saturated porous layer, Cross-diffusion effects, *European J. B/Fluids* 65 (2017) 70–87.
[33] J. Prathap Kumar, J.C. Umavathi, C.K. Murthy, Double diffusive convection of porous matrix saturated with nanofluid, Int. J. Engng. Sci. and Research 5 (2017) 11–43.
[34] J.C. Umavathi, B. Buonomo, O. Manca, M.A. Sheremet, Double diffusion in rectangular duct using metals or oxides suspended in a viscous fluid, Thermal Science and Engineering Progress 21 (2021), 100793.
[35] A.A. Yinusa, M.G. Sobamowo, M.A. Usman, E.H. Abubakar, Exploration of three dimensional squeezed flow and heat transfer through a rotating channel with coupled Dufour and Soret influences, Thermal Science and Engineering Progress 21 (2021) 100788, https://doi.org/10.1016/j.tsep.2020.100788.
[36] K.S. Al Kalbani, M.M. Rahman, M. Ziad Saghir, Entropy generation in hydromagnetic nanofluids flow inside a tilted square enclosure under local thermal nonequilibrium condition, Int. J. Thermofluids 5-6 (2020) 100031, https://doi.org/10.1016/j.ijft.2020.100031.
[37] M.Z. Saghir, M.M. Rahman, Brownian motion and thermophoretic effects of flow in channels using nanofluid: A two-phase model, Int. J. Thermofluids 10 (2021) 100085, https://doi.org/10.1016/j.ijft.2021.100085.
[38] R.D. Plant, M.Z. Saghir, Numerical and experimental investigation of high concentration aqueous alumina nanofluids in a two and three channel heat exchanger, Int. J. Thermofluids 9 (2021) 100055, https://doi.org/10.1016/j.ijft.2020.100055.
[39] V. Bianco, B. Buonomo, A. di Pasqua, O. Manca, Heat transfer enhancement of laminar impinging slot jets by nanofluids and metal foams, Thermal Science and Engineering Progress 22 (2021) 100860, https://doi.org/10.1016/j.tsep.2021.100860.
[40] D. Srinivasacharya, K.S. Ramana, Thermal radiation and double diffusive effects on bioconvection flow of a nanofluid past an inclined wavy surface, Thermal Science and Engineering Progress 22 (2021) 100830, https://doi.org/10.1016/j.tsep.2020.100830.
[41] T. Tayebi, H.F. Öztop, A.J. Chamkha, Natural convection and entropy production in hybrid nanofluid filled-annular elliptical cavity with internal heat generation or absorption, Thermal Science and Engineering Progress 19 (2020) 100605, https://doi.org/10.1016/j.tsep.2020.100605.
[42] V. Javeri, Analysis of laminar thermal entrance region of elliptical and rectangular channels with Kantorowich method, Warme Stoffuberragung 9 (2) (1976) 85–98.
[43] V. Javeri, Heat transfer in laminar entrance region of a flat channel for the temperature boundary condition of the kind, Warme Stoffubertragung Thermo Fluid Dyn. 10 (1977) 137–144.
[44] V. Javeri, Laminar heat transfer in a rectangular channel for the temperature boundary condition of the third kind, Int. J. Heat Mass Transfer 21 (8) (1978) 1029–1034.
[45] J.C. Umavathi, J. Prathap Kumar, J. Sultana, Mixed convection flow in a vertical porous channel with boundary conditions of third kind with heat source/sink, J. Porous Media 15 (2012) 998–1007.
[46] Umavathi, J.C., Prathap Kumar, J., and Jaweriya Sultana, Mixed convection flow in a vertical channel with boundary conditions of the third kind in the presence of heat source/sink, Appl. Math. Mech.-Engl. Ed., 2012b, 33, pp. 1015–1034.
[47] J.C. Umavathi, J. Sultana, Mixed convective flow of micropolar fluid mixture in a vertical channel with boundary conditions of third kind, J. Engn. Phys. and ThermoPhysics 85 (2012) 895–908.
[48] J.C. Umavathi, A.J. Chamkha, Fully developed mixed convection in a vertical channel in the presence of heat source or heat sink, Int. J. Energy and Technology 3 (2011) 1–9.
[49] J.C. Umavathi, A.J. Chamkha, Mixed convection flow of an electrically-conducting fluid in a vertical channel with boundary conditions of the third kind, Canadian Journal of Physics 92 (11) (2014) 1387–1396.
[50] J.C. Umavathi, M.A. Sheremet, Influence of temperature dependent conductivity of a nanofluid in a vertical rectangular duct, Int. J. Nonlinear Mechanics 78 (2016) 17–28.
[51] J.C. Umavathi, M.A. Sheremet, Mixed convection flow of an electrically conducting fluid in a vertical channel using Robin boundary conditions with heat source or sink, Eur. J. of Mechanics B. Fluids 55 (2016) 132–145.
[52] Gebhart, B., Jaluria, Y., Mahajan, R.L., and Sammakia, B., Buoyancy-induces flows and Transport, New York, NY: Hemisphere, 1988.
[53] E. Zanchini, Effect of viscous dissipation on mixed convection in a vertical channel with boundary conditions of third kind, Int. J. Heat Mass Transfer 41 (1988) 3949–3959.
[54] F.C. Lai, F.A. Kulacki, Non-Darcy convection from horizontal permeable surfaces in saturated porous media, Int. J. Heat Mass Transfer 30 (1987) 2198–12192.